Inorganic Chemistry

Article

pubs.acs.org/IC

Lithiation-Induced Zinc Clustering of Zn_3, Zn_{12}, and Zn_{18} Units in Zintl-Like $Ca_{\sim 30}Li_{3+x}Zn_{60-x}$ (x = 0.44−1.38)

Qisheng Lin*

Division of Materials Science and Engineering, Ames Laboratory, U.S. Department of Energy, Ames, Iowa 50011 United States

Supporting Information

ABSTRACT: Zinc clusters are not common for binary intermetallics with relatively low zinc content, but this work shows that zinc clustering can be triggered by lithiation, as exemplified by $Ca_{\sim 30}Li_{3+x}Zn_{60-x}$, $P6/mmm$, Z = 1, which can be directly converted from $CaZn_2$. Two end members of the solid solution (x = 0.44 and 1.38) were established and structurally characterized by single-crystal X-ray diffraction analyses: $Ca_{30}Li_{3.44(6)}Zn_{59.56(6)}$, a = 15.4651(9) Å, c = 9.3898(3) Å; $Ca_{30.45(2)}Li_{4.38(6)}Zn_{58.62(6)}$, a = 15.524(3) Å, c = 9.413(2) Å. The structures of $Ca_{\sim 30}Li_{3+x}Zn_{60-x}$ feature a condensed anionic network of Zn_3 triangles, lithium-centered Zn_{12} icosahedra, and *arachno*-$(Zn,Li)_{18}$ tubular clusters that are surrounded respectively by Ca_{14}, Ca_{20}, and Ca_{30} polyhedra. These polyhedra share faces and form a clathrate-like cationic framework. The specific occupation of lithium in the structure is consistent with theoretical "coloring" analyses. Analysis by the linear muffin-tin orbital (LMTO) method within the atomic sphere approximation reveals that $Ca_{\sim 30}Li_{3+x}Zn_{60-x}$ is a metallic, Zintl-like phase with an open-shell electronic structure. The contribution of Ca−Zn polar covalent interactions is about 41%.

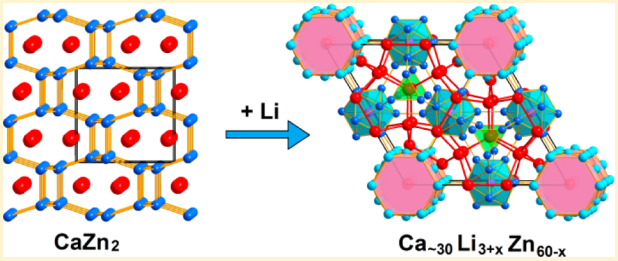

INTRODUCTION

Within the Periodic Table, 80% of the elements are metals. Therefore, it is not surprising that metal−metal bonding plays a central role for molecular and solid-state chemistry. Metal clusters exist for transition metals and main-group metals and could be naked, interlinked, or stabilized by ligands.[1−4] In general, main-group clusters are often seen in Zintl phases, in which electropositive metals are assumed to donate all valence electrons to the electronegative components coming near the so-called Zintl border.[5] The stability and structures of Zintl phases can be generally rationalized by the Wade−Mingos rule[6,7] and/or the Zintl−Klemm−Busmann concept.[8,9] For transition-metal clusters, later transition metals with low oxidation states or early transition metals with middle oxidation states are more popular, and their structures can be rationalized by the polyhedral skeletal electron pair theory originating from Wade−Mingos rules.[10]

Metal clusters of group 12 elements (Zn, Cd, and Hg) occur relatively less frequently than those of its neighboring group 11 (Cu, Ag, and Au) and group 13 (B, Al, Ga, In, and Tl) elements. The reason is related to the $d^{10}s^2$ closed-shell atomic configurations of group 12 elements and large energy gaps between their s and p valence orbitals.[11] Therefore, effective s−p orbital mixing for group 12 elements can only be accomplished by forming large clusters so that s and p orbitals become more dispersive. Two possible routes to achieving such large clusters of group 12 elements are (1) to combine with elements on the Zintl border, i.e., Ga, In, and Tl, which tend to form clusters, as seen in the ternary phases $M_8(Ga,Zn)_{41}$ (M = V, Cr, Mn)[12] and (2) to target compounds with high percentages of group 12 elements, such as $Ce_{13}Zn_{58}$, $La_{13}Hg_{58}$, $ScZn_6$, $CaCd_6$, Dy_2Zn_{17}, $BaCd_{11}$, $NaZn_{13}$, and KCd_{13}.[13] In contrast, binaries with relatively lower percentages of group 12 elements generally exhibit network structures, e.g., $CaCd_2$, Ca_5Zn_3, and Ba_2Hg.[13]

In the past decade, intermetallics containing clusters of group 12 elements have attracted considerable interest in the research of quasicrystals and approximants.[14−22] Particularly, MCd_6 (M = Ca, Yb) have been the model systems for chemical tuning[23] of new Tsai-type quasicrystals and approximants since the discovery of $MCd_{5.67}$ quasicrystals in 2000.[24] For example, an icosahedral quasicrystal $Sc_{16.2}Cu_{12.3}Zn_{71.5}$[14] and its corresponding $Sc_3Cu_yZn_{18-y}$ (y = 0−2.2) crystalline approximants[15] have been discovered in the zinc-rich region of the Sc−Cu−Zn phase triangle. Recently, interesting structural and bonding phenomena have been found among valence-electron-poor, polar intermetallics containing group 12 elements, especially those containing gold or platinum. For instance, the tunnel-like structures of $Na_{0.97}Au_2Zn_4$ and $Na_{0.72}Au_2Zn_2$ are respectively the 1 × 1 × 3 superstructure and an incommensurately modulated derivative (with a modulation vector q = 0.189 along c) of $K_{0.37}Cd_2$, although both structures feature layers of gold or zinc squares that are condensed antiprismatically along c.[25] The structure of the Mn_6Th_{23}-type $Na_6Cd_{16}Au_7$ consists of Cd_8 tetrahedral stars that are face-capped by six shared gold vertexes and further diagonally bridged via another gold to generate an

Special Issue: To Honor the Memory of Prof. John D. Corbett

Received: September 24, 2014
Published: November 14, 2014

   dx.doi.org/10.1021/ic502326j | Inorg. Chem. 2015, 54, 922−929

orthogonal, three-dimensional framework $[Cd_8(Au)_{6/2}(Au)_{4/8}]$.[26] Segregation of homoatomic clusters of group 12 elements is very impressive in the structure of $Na_6Cd_{16}Au_7$. Similar homoatomic tetrahedral star clustering phenomena is also observed in $Ca_6Pt_8Cd_{16}$.[27] In contrast, novel cadmium clustering occurs in the structure of Ca_6PtCd_{11},[28] which contains Cd_7 pentagonal bipyramids, linear cadmium arrays, and rectangular Cd_4Pt pyramids.

Of particular interest in this work is the chemistry of zinc clusters in intermetallic phases. On the one hand, novel intermetallic structures containing group 12 elements are necessary for the evaluation, rationale, and possibly new development of relationships between clusters and the valence electron count (VEC) in the case when Wade−Mingos rules and the Zintl concept fall short. On the other hand, rechargeable zinc batteries are attracting increased attention because of their advantages in safety, low cost, environmental friendliness, and flexibility.[29] However, the formation of zinc dendrites on electrodes during charge−discharge cycles is a major reason for the short lifetime of these batteries.[30,31] Computer simulations have shown that zinc dendrites could grow from small clusters Zn_n ($n \geq 2$).[32,33] However, there are no as yet proven examples among inorganic complexes or intermetallic compounds for the geometries of most Zn_n clusters used for simulations. Herein, the structure of $Ca_{\sim 30}Li_{3+x}Zn_{60-x}$ (x = 0.44−1.38) containing an extended network of Zn_3 triangles, Zn_{12} icosahedra, and $(Li,Zn)_{18}$ tubular clusters is reported, together with analyses of bonding, coloring, and a rationale using classical valence electron counting schemes. Similar zinc-dominated structural motifs, including nickel-centered Zn_{12} icosahedra and Ni_6Zn_{12} tubular clusters, have only been reported for $(Yb,Ca)_{32}Ni_9Zn_{54}$.[34] The composition of the title phase is close to the $CeCu_2$-type $CaZn_2$, in which zinc forms a three-dimensional network rather than clusters. However, the presence of a small amount (~4 mol %) of lithium leads to a drastic structural change to an extended network of Zn_n clusters.

EXPERIMENTAL SECTION

Syntheses. All reactants, including dendritic calcium pieces (99.95%), lithium ingot (99.9%), copper powder (99.9%), and zinc shot (99.99%), all from Alfa Aesar, were handled inside an argon-filled glovebox (≤0.1 ppm of H_2O by volume). The weighed reactants (~400 mg in total) were sealed inside tantalum tubes that were subsequently sealed in an evacuated silica jacket. Samples were heated to 700 °C at a rate of 120 °C/h, held there for 2 h, cooled to 400 °C at a rate of 5 °C/h, annealed for 1 week, and then quenched in water.

The title phase was first obtained in a reaction with nominal composition "$CaLi_2Zn_2$", which produced a mixture of the title phase $Ca_{30.45(2)}Li_{4.69(6)}Zn_{58.31(6)}$ (refined from single-crystal data) and lithium. Subsequently, reactions loaded as $Ca_{30.5}Li_xZn_{63-x}$ (x = 1, 3, 5, and 10) were reacted under the same reaction conditions. Phase analyses using powder X-ray diffraction (XRD) indicated a pure phase product of the title phase for the x = 5 reaction. For reactions with x = 1 and 3, mixtures of the title phase and $CaZn_2$ were obtained; for x = 10, a mixture of ~90% title phase and an unknown phase was seen.

A separate reaction of $CaZn_2$ in the absence of lithium was also run under the same reaction conditions, and a pure $CeCu_2$-type $CaZn_2$ phase was produced. However, a mixture of $CaZn_2$ (mp 705 °C) and lithium in a mole ratio of 6:1 (equal to "$Ca_{30}Li_5Zn_{60}$") reacted under the foregoing reaction conditions produced high yields (>95%) of the title phase. In contrast, the reaction of "$Ca_{30}Cu_5Zn_{60}$" to see if copper can replace lithium to form the same phase produced just the solid solution $Ca(Cu,Zn)_2$.

The title phase is brittle, shiny with a metallic luster, and inert to air at room temperature for at least 12 months. Crystals are also stable in water. Single-crystal X-ray structural analysis of a crystal that had been immersed in water for 2 h revealed no structural and composition changes. The remarkable stability of the product in air and water may be ascribed to the fact that a majority of lithium in the structure is encapsulated by Zn_{12} icosahedral clusters, whereas the remaining lithium is mixed with zinc to form a covalently bonded anionic network.

Phase Analyses. Phase analyses were carried out using both powder and single-crystal XRD. Powder XRD measurements on crushed polycrystalline samples were performed at room temperature using a STOE Stadi P powder diffractometer equipped with an image plate and Cu Kα_1 radiation (λ = 1.5406 Å). A small amount (~10% by volume) of silicon standard (NIST 640b) powder was added to each fine powder sample so that the peak positions could be consistently calibrated in refinements of the lattice parameters. Each powder sample was dispersed between two acetate films with the aid of a small amount of grease.

Single-crystal XRD data were collected at room temperature using a Bruker SMART APEX II diffractometer equipped with Mo Kα radiation (λ = 0.71073 Å) over a 2θ range of ~3°−60° in mixed ω and φ scan modes and exposures of 10 s/frame. Intensity data were integrated with the *SAINT* program.[35] Empirical absorption corrections were made with the aid of *SADABS*.[36] The space group *P6/mmm* was suggested by absence analyses with the aid of *XPREP* in *SHELXTL 6.1*.[37] The program *Superflip*[38] was employed to set up the initial structural models, and then the models were transferred to the *SHELXTL* program for least-squares refinements and further analyses.

Single-Crystal Structural Analyses. The structures of five single crystals from products of different reactions were solved, with refined compositions summarized by the formula $Ca_{\sim 30}Li_{3+x}Zn_{60-x}$. Because all structures are quite similar, with small differences in the Zn/Li occupancy ratios and calcium disorder in tunnels, herein only the two end members, i.e., $Ca_{30}Li_{3.44(6)}Zn_{59.56(6)}$ (**1**) and $Ca_{30.45(2)}Li_{4.38(6)}Zn_{58.62(6)}$ (**2**) will be presented, and the structural solution of crystal **1** is taken as an example.

For crystal **1**, a total of six Zn atoms and five Ca atoms with reasonable interatomic distances were obtained by *Superflip*;[38] thus, they were respectively assigned to Zn1−Zn6 and Ca1−Ca5 sites. After a few cycles of least-squares refinements in *SHELXTL*,[37] R1 converged at 5.89% and the difference Fourier map indicated only the special site ($^1/_2$, 0, $^1/_2$) can be assigned to lithium, judging from its peak height and distance to the neighboring Zn1 site (2.58 Å). Subsequent refinements including lithium converged smoothly to R1 = 5.76%. At this stage, Zn3 and Zn5 had slightly large isotropic displacement parameters (U_{eq} = 0.021 Å^2 for both) compared to the other Zn atoms (0.010−0.013 Å^2), an indication of Zn/Li mixtures for both sites. In addition, the U_{eq} value (0.106 Å^2) of Ca5 was about 10 times larger compared to other Ca atoms (0.012−0.016 Å^2). However, separate refinements to check possible Ca/Li mixing at the Ca5 site indicated full occupation by calcium, suggesting that the large U_{eq} value must be incurred from other reasons (see below). So, Zn/Li mixtures were assigned at the foregoing Zn3 and Zn5 sites in subsequent refinements with anisotropic displacement parameters for all Zn and Ca atoms. The refinements converged at R1 = 2.94% and wR2 = 6.58% with GOF on F^2 of 1.118 for 56 parameters and 1171 observed reflections [$I > 2\sigma(I)$], resulting in the refined composition $Ca_{30}Li_{3.44(6)}Zn_{59.56(6)}$ for **1**.

The maximal and minimal residual peaks in the difference Fourier map of crystal **1** are 3.820 e/Å^3 (0.01 Å from Ca5) and −4.427 e/Å^3 (0.68 Å from Ca5); both peaks arise from the imperfect description of the elongated electron density at the Ca5 site (U_{33}:U_{11}:U_{22} = 0.944:0.012:0.0122). In this case, refinements with Ca5 replaced by two split positions, (0, 0, 0.2687) and (0, 0, 0.1658) as suggested by *SHELXTL*,[37] were always unstable because of the divergence of z coordinates. If z coordinates of the two parts were fixed, each part was suggested to split again, and so on. Therefore, the structure was preferred to refine with large **U** tensors rather than refine with split positions. Similar phenomena were also found in several tunnel

dx.doi.org/10.1021/ic502326j | *Inorg. Chem.* 2015, 54, 922−929

structures such as $Na_{30.5}Ag_{2.6}Ga_{57.4}$,[39] $Na_{30.1}Au_{3.4}Ga_{56.6}$,[40] and $Na_{0.97}Au_2Zn_4$ and $Na_{0.72}Au_2Zn_2$.[25]

The structure solution of crystal **2** was quite similar to that of **1**, except that the Ca5 site could be evidently represented by two parts, and an additional partially occupied Ca6 site was assigned to represent the electron density at the origin. As a result, the difference Fourier map was smooth (±2.4 e/Å^3). All refined positions of these disordered atoms fit very well to the observed electron density map (below).

Details of data collection and structural refinements for crystals **1** and **2** are summarized in Table 1. Atomic positions and equivalent isotropic displacement parameters are given in Table S1 and selected interatomic distances in Table S2, both in the SI. Anisotropic thermal factors and other detailed crystallographic data are given in the CIF file in the SI. It is worth mentioning that techniques such as energy-dispersive X-ray and inductively coupled plasma spectroscopies, which are often used to examine chemical compositions, are disfavored to detect lithium in the present phases. Li^7 NMR is also not a good choice because the crystals exhibit metallic conductivity, and there are three independent sites involving lithium in the structure, which makes the separation of the respective signals very difficult. Because the refined composition range ($Ca_{30.25\pm0.25}Li_{3.91\pm0.47}Zn_{59.09\pm0.47}$) is very close to the loaded composition "$Ca_{30.5}Li_5Zn_{58}$", which produced a pure phase product according to powder XRD, no other measurement was attempted to confirm this refined composition, including neutron diffraction data, which could help to obtain a more accurate lithium composition, in theory, while forfeiting the accuracy of other elements.

Table 1. Crystal Data and Structure Refinement for $Ca_{30}Li_{3.44(6)}Zn_{59.56(6)}$ and $Ca_{30.45(2)}Li_{4.38(6)}Zn_{58.62(6)}$

	1	2
empirical formula	$Ca_{30}Li_{3.44(6)}Zn_{59.56(6)}$	$Ca_{30.45(2)}Li_{4.38(6)}Zn_{58.62(6)}$
fw	5119.71	5082.82
space group, Z	$P6/mmm$, 1	$P6/mmm$, 1
unit cell dimensions		
a (Å)	15.4651(9)	15.524(3)
c (Å)	9.3898(6)	9.413(2)
V (Å^3)	1944.9(3)	1964.6(9)
d_{calcd} (g/cm^3)	4.371	4.296
abs coeff (mm^{-1})	19.936	19.486
reflns collect/R_{int}	27883/0.0761	25369/0.1097
data/restraints/param	1171/0/56	1087/0/63
GOF	1.118	1.027
R1/wR2 [$I > 2\sigma(I)$]	0.0294/0.0658	0.0296/0.0552
R1/wR2 (all data)	0.0460/0.0720	0.0548/0.0616
max/min peaks (e/Å^3)	3.820/−4.427	2.397/−2.359

Electronic Structure Calculations. Tight-binding calculations on hypothetical model "$Ca_{30}Li_3Zn_{60}$" were performed self-consistently using the linear muffin-tin orbital (LMTO) method within the atomic sphere approximation (ASA).[41−43] Scalar relativistic corrections were included. The radii of the Wigner−Seitz (WS) spheres were assigned automatically so that the overlapping potentials would be the best possible approximations to the full potentials. The WS radii (Å) were automatically scaled by the program: Ca, 1.85−1.99; Li, 1.39; Zn, 1.40−1.52. No additional empty spheres were inserted subject to the overlap restriction of 16% for atom-centered WS spheres. Basis sets of Ca 4s3d (4p), Li 2s (2p), and Zn 4s4p wave functions were employed, with downfolded orbitals in parentheses. Reciprocal space integrations were carried out using the tetrahedron method. Crystal orbital Hamilton populations (COHPs)[44] for selected atom pairs were calculated. From these COHP analyses, the contribution of the covalent part of a particular interaction to the total bonding energy of the crystal can be obtained. The weighted integration of COHP up to E_F, i.e., −ICOHP, is an indicator of the relative bond strengths.

To establish valence-electron-counting rules of the title phase, molecular orbitals (MOs) of isolated $Li@Zn_{12}H_{12}^{13-}$ and $Zn_{18}H_{12}^{18-}$ polyhedra were calculated by the extended Hückel tight-binding (EHTB) method using *CAESAR for Windows*.[45] Each cluster exobond was simulated by placing a H atom with an orbital energy of Zn 4p. Orbital energies (H_{ii}), exponents (λ), and coefficients (ξ) employed in the calculation are Zn 4s, H_{ii} = −12.41 eV, λ = 2.01, ξ = 1.00; 4p, H_{ii} = −6.53 eV, λ = 1.70, ξ =1.00; 3d, H_{ii} = −15.00 eV, λ_1 = 5.95, ξ_1 = 0.5933, λ_2 = 2.30, ξ_2 = 0.5846.

Resistivity Measurements. A piece of polycrystalline sample from the "$Ca_{30.5}Li_5Zn_{58}$" reaction (X-ray pure phase) was mechanically polished into a cuboid for electrical resistivity measurement by the four-probe method. Resistivity data were collected using a Quantum Design Physical Measurement System (PPMS) within the temperature range of 2−300 K. For comparison, resistivity data of a high-quality single crystal of $CaZn_2$ in a cuboid shape were also collected.

RESULTS AND DISCUSSION

Lithiation of $CaZn_2$. Zinc clusters are not popular in both molecular complexes and intermetallic materials because of the closed-shell configuration of zinc ($3d^{10}4s^2$) and its large energy gap (4 eV)[11] between 4s and 4p orbitals. To form zinc clusters, viz., to achieve effective s−p orbital mixings, a high percentage of zinc is usually necessary. For Ca−Zn binaries, zinc clusters only form when the zinc percentage is at least 75 mol %, such as $CaZn_3$, $CaZn_5$, and $CaZn_{11}$, whereas for binaries with lower zinc percentages, a three-dimensional network ($CaZn_2$), a *zigzag* chain (CaZn), Zn_2 dimers (Ca_5Zn_3), or isolated Zn atoms (Ca_3Zn) are found.

Because the composition of the title phase $Ca_{\sim30}Li_{3+x}Zn_{60-x}$ (x = 0.44−1.38) is close to Ca:Zn = 1:2, an independent reaction of $30CaZn_2$ + 5Li → "$Ca_{30}Li_5Zn_{60}$" was designed to check whether lithiation could occur directly from the binary compound. The XRD pattern indicated a high yield (>95%) of the title phase. Therefore, it is safe to conclude that the formation of various Zn_n (n = 3, 12, 18) clusters is triggered by the presence of a small percentage of lithium (∼4 mol %). However, how the three-dimensional framework of zinc in $CaZn_2$ transforms into an extended network of condensed clusters is not known yet.

Structure. The structures of **1** and **2** are very similar, except that (1) the Ca5 site has very diffuse electron density in **1**, but the corresponding atom in **2** splits into two separated parts (see Figure 1) and (2) the Wyckoff 1a (0, 0, 0) site, which is the center of a M_{18} tubular cluster, is empty in **1**, and it is occupied by Ca6 with a refined occupancy of 45.7(6)% in **2**. Split sites were also found for some other related structures containing tunnels, e.g., $Na_{30.5}Ag_{2.6}Ga_{57.4}$,[39] but, in general, the total number of atoms in tunnels is less than 3 per formula. The exception is $Ca_{24.7}Yb_{6.7}Ni_9Zn_{54}$,[46] in which, however, the 3.4 Ca atoms in the tunnel (cf. Table 2) could be refined as 1.62Ca + 0.51Yb if the average Ca/Yb ratio is kept the same as that of other Ca/Yb mixed sites. Highly disordered atoms in tunnels are often found, e.g., $Na_{0.72}Au_2Zn_2$,[32] KAu_4In_2,[47] Mn_3Si_5-type structures,[48] and $Sc_4Mg_xCu_{15-x}Ga_{\sim7.5}$.[49] Such positional disorders are related to both the size and geometry of the tunnels as well as the size of atoms sitting in the tunnels. Atoms in straight tunnels are usually more diffuse than those in a tunnel with varied sizes along the tunnel direction. Sometimes the latter type tunnel might contain well-defined sites for atoms inside the tunnel (e.g., KAu_4In_2[47]), and sometimes it might result in incommensurately modulated structures, e.g., $Na_{0.72}Au_2Zn_2$[25] and $Sc_4Mg_xCu_{15-x}Ga_{\sim7.5}$.[49] In the following, given the similarities between crystals **1** and **2**, crystal **1** is selected for structural description.

The Pearson symbol for **1** is *hP*93 with the prototype ascribed to $Ca(Cu,Al)_{2.1}$.[50] As shown in Figure 2, the structure

dx.doi.org/10.1021/ic502326j | Inorg. Chem. 2015, 54, 922−929

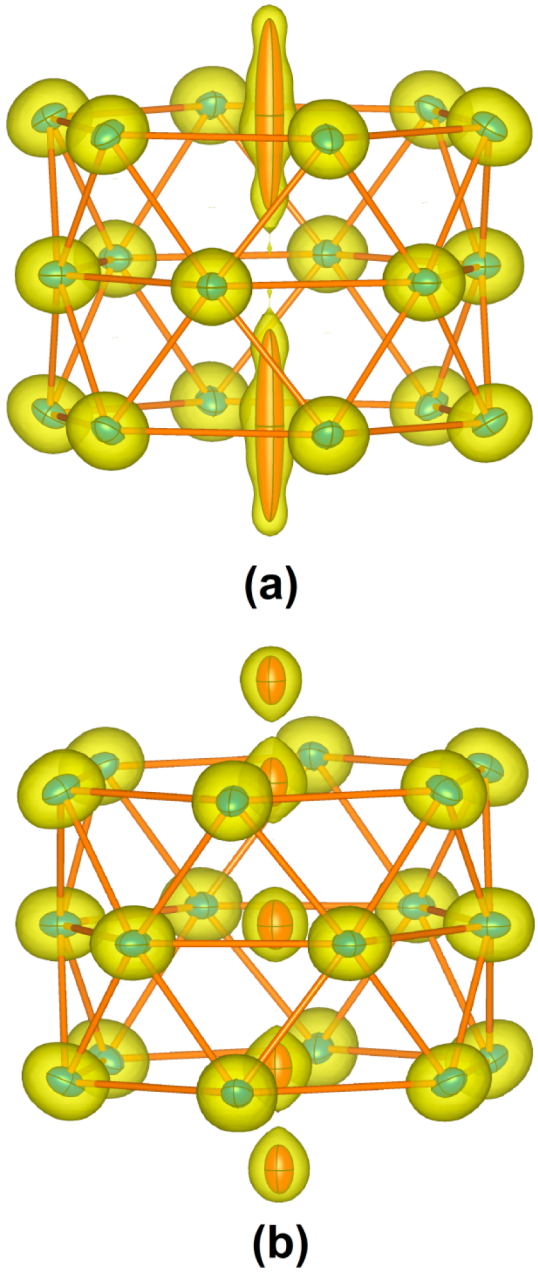

Figure 1. Observed electron densities (yellow) about *arachno*-M_{18} tubular clusters in (a) $Ca_{30}Li_{3.44(6)}Zn_{59.56(6)}$ and (b) $Ca_{30.45(2)}Li_{4.38(6)}Zn_{58.62(6)}$, with an isosurface cutoff level at 6 e/Å^3. Ellipsoids representing Ca (red) and M (blue) at 50% probability are overlaid.

features a clathrate-like framework (red) that is defined by the most electropositive Ca atoms and is composed of Ca_{20} dodecahedra (or 5^{12} using the Schäfli notation of clathrate structures), Ca_{30} polyhedra ($3^{12}5^{12}6^2$), and Ca_{14} polyhedra (3^65^6), all face-shared, in the corresponding ratio of 3:1:2. However, the packing of these cationic polyhedra does not form any known type of clathrate structure.[51] These three different polyhedra encapsulate, respectively, lithium-centered Zn_{12} icosahedral clusters (shaded in turquoise), *arachno*-M_{18} (M = Zn/Li) tubular clusters (rose), and Zn_3 triangular clusters (green). The three types of anionic clusters are interconnected via two-center, two-electron (2c-2e) intercluster bonding to form a three-dimensional extended network. The *arachno*-M_{18} tubular clusters stack on each other with a separation equal to the *c* lattice constant, resulting in the formation of large tunnels parallel to the *c* axis. There is no Ca atom sitting at the exact middle point (z = 0.5) of two adjacent M_{18} tubular clusters; otherwise, a short distance from the Ca2 sites, which form hexagonal rings lying at z = 0.5 (cf. Figures 1 and 3), would result. Therefore, a common formula for **1** and **2** can be expressed as $Ca_{28}(Ca_{2+\Delta})(Li@Zn_{12})_3(Zn_{18-x}Li_x)(Zn_3)_2$ according to their structural units: a clathrate-like framework of Ca_{28}, three $Li@Zn_{12}$ icosahedra, one *arachno*-M_{18} tubular cluster filled with the linear chain $Ca_{2+\Delta}$, and two Zn_3 triangles.

The $Li@Zn_{12}$ icosahedral cluster (Figure 3a) is defined by three Zn1, three Zn2, and three Zn4 atoms. Each Zn1 atom in this icosahedron is bonded to another Zn1 atom of an adjacent icosahedron, whereas each Zn2 is bonded to Zn6 of a neighboring Zn_3 triangle, and each Zn4 is bonded to a M3 atom of a neighboring *arachno*-M_{18} cluster. The intracluster Zn−Zn distances within the icosahedron vary from 2.710(2) to 2.8346(7) Å (see Table S2 in the SI) with a weighted average of 2.78(1) Å. In comparison, the intercluster Zn−Zn distance ranges from 2.585(2) to 2.7724(9) Å, with an average of 2.67(1) Å, which is close to the sum of Pauling's metallic radius of zinc, 2.678 Å.[52] These facts suggest that the intercluster bonds adopt typical 2c-2e bonding, whereas intracluster bonding is more delocalized, i.e., multicentered. The strength of inter- and intracluster bonding can be estimated by −ICOHP data (Table S2 in the SI). On average, the intercluster Zn−Zn bonding is at least 30% stronger than intracluster Zn−Zn bonding. All Zn_{12} icosahedra are centered by a Li atom, with center-to-vertex distances falling in the range of 2.5757(7)−2.7042(7) Å. These distances are comparable to related bonds in NaTl-type LiZn (2.689 Å)[53] and $MgCu_2$-type Mg_2LiZn_3 (2.612−2.625 Å).[46] The average −ICOHP value for Li−Zn bonds is about 0.20 eV/bond, which is smaller than the average of Ca−Zn bonds (0.45 eV/bond). Each $Li@Zn_{12}$ icosahedron is surrounded by a Ca_{20} dodecahedron that is defined by eight Ca1, four Ca2, four Ca3, and four Ca4 atoms. The assembly $Li@Zn_{12}@Ca_{20}@Zn_8M_4$ is a typical mini-Bergman cluster, which is commonly seen in the so-called Bergman-type phases.[54]

It is worth mentioning that about 87.2% (=3/3.44) of the Li atoms in crystal **1** are located at the center of the Zn_{12} icosahedra, and the remaining 12.8% of the Li atoms are directed to the M_{18} tubular cluster. This tubular cluster (Figure 3b) is an *arachno*-M_{18} polyhedron defined by 12 M3 and 6 M5 atoms, which form three hexagonal rings stacked along the *c* axis, with the ring of 6 M5 atoms being the waist. The M3−M5 distance is 2.5966(6) Å (Table S2 in the SI). In contrast, other distances in the tubular cluster (M3−M3 and M5−M5) exceed 3.0 Å, suggesting barely any bonding interaction. In this tubular cluster, each M5 atom at the waist has no exobond, but each M3 atom is exobonded to the Zn4 atom of neighboring Zn_{12} icosahedra. The centers of two hexagonal faces of the M_{18} tubular cluster are occupied by Ca atom(s), either ordered or disordered. Also, each M_{18} cluster is enclosed by a Ca_{30} polyhedron, which exhibits 12 triangles, 12 pentagons, and 2 hexagonal faces (thus denoted as $3^{12}5^{12}6^2$). Each of the 12 pentagonal faces of Ca_{30} is intersected orthogonally by a M3−Zn4 exobond of the M_{18} tubular cluster (Figure 3b).

The Zn_3 triangular cluster (Figure 3c) is generated by Zn6 atoms. The Zn6−Zn6 distance is 2.851(2) Å, which is the longest Zn−Zn distance in this structure. Each Zn6 site form two exobonds to Zn2 atoms with a distance of 2.7724(9) Å,

dx.doi.org/10.1021/ic502326j | *Inorg. Chem.* 2015, 54, 922−929

Table 2. Comparison of Phases with Structural Motifs Similar to That of the Title Phase $Ca_{\sim 30}Li_{3+x}Zn_{60-x}$

phase	formulation based on structural units	c/a	VEC	r_{ico} (Å)	ref
$Ca_{30}Li_{3.44}Zn_{59.56}$	$Ca_{28}(Ca_2)(Li@Zn_{12})_3(Zn_{17.56}Li_{0.44})(Zn_3)_2$	0.608	182.6	2.643	this work
$Ca_{30.45}Li_{4.38}Zn_{58.62}$	$Ca_{28}(Ca_{2.45})(Li@Zn_{12})_3(Zn_{16.62}Li_{1.38})(Zn_3)_2$	0.606	182.5	2.650	this work
$Ca_{24.7}Yb_{6.7}Ni_9Zn_{54}$	$(Ca_{21.3}Yb_{6.7})(Ca_{3.4})[Ni@(Zn_{12})]_3(Ni_6Zn_{12})(Zn_3)_2$	0.606	188.8	2.612	34
$Ba_{30.3}Li_{33.6}In_{29.4}$	$Ba_{28}(Ba_{2.3})(Li@In_{6.5}Li_{5.5})_3(In_{5.9}Li_{12.1})(In_{2.0}Li_{1.0})_2$	0.610	182.4	2.939	53
$Ca_{30}Cu_{29.46}Al_{33.68}$	$Ca_{28}(Ca_2Cu_{0.05}Al_{0.15})[Cu@(Cu_{5.35}Al_{6.65})]_3(Cu_{9.72}Al_{8.28})(Cu_{0.3}Al_{2.4})_2$	0.606	190.5	2.593	63
$Ca_{30}Cu_{25.0}Al_{38.0}$	$Ca_{28}(Ca_2)[Cu@(Cu_{4.33}Al_{7.67})]_3(Cu_9Al_9)(Al_3)_2$	0.607	199.0	2.596	50
$Na_8K_{23}Cd_{12}In_{48}$	$(Na_6K_{22})(Na_2K)(\square@In_{12})_3(Cd_{12}In_6)(In_3)_2$	0.610	199.0	2.918	61
$Na_{30.5}Ag_{6.4}Ga_{53.6}$	$Na_{28}(Na_{2.5})(\square@Ga_{12})_3(Ga_{11.6}Au_{6.4})(Ga_3)_2$	0.612	197.7	2.597	39
$Na_{30.5}Ag_{2.6}Ga_{57.4}$	$Na_{28}(Na_{2.5})(\square@Ga_{12})_3(Ga_{15.7}Au_{2.6})(Ga_3)_2$	0.611	205.3	2.597	39
$Na_{30.1}Au_{3.4}Ga_{56.6}$	$Na_{28}(Na_{2.1})(\square@Ga_{12})_3(Ga_{12.64}Au_{5.36})(Ga_3)_2$	0.601	203.3	2.640	40
$Na_{6.0}Mg_{24.0}Ga_{55.2}$	$(Mg_{22.4}Na_{5.6})(Mg_{1.6}Na_{0.4})(\square@Ga_{12})_3(Ga_{13.2}\square_{4.8})(Ga_3)_2$	0.583	219.6	2.611	60

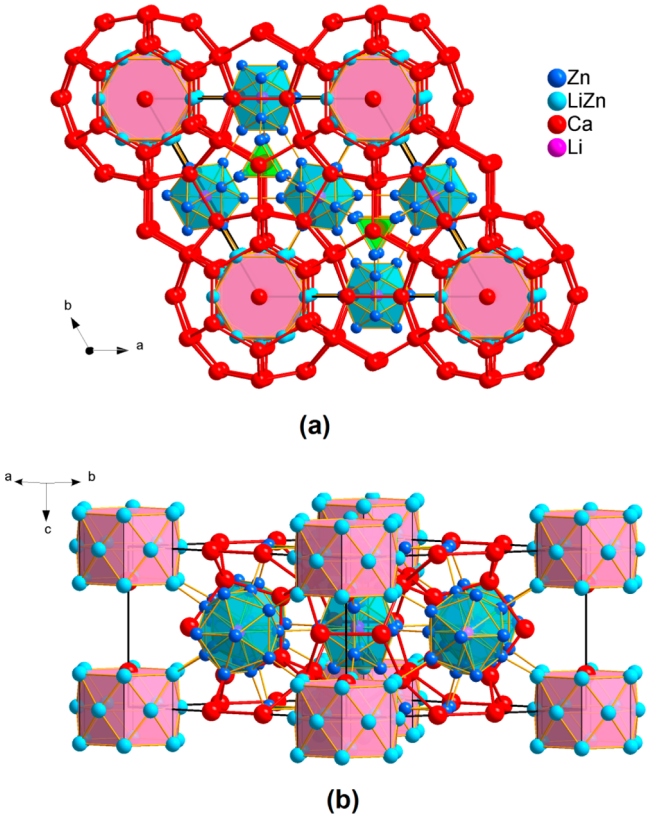

Figure 2. Cluster representations of a unit cell of **1** projected along the (a) (001) and (b) (110) directions. For clarity, Ca atoms beyond the unit cell in part a are not shown in part b.

and each exobond is perpendicular to a pentagonal face of the encapsulating Ca_{14} polyhedron (3^65^6).

Coloring. As refined from single-crystal data (Table S1 in the SI), the centers of icosahedra in the title phase are exclusively occupied by Li atoms and only the M3 and M5 sites are occupied by Zn/Li mixtures, whereas Zn1, Zn2, Zn4, and Zn6 sites that generate icosahedral and triangular clusters are free of lithium. To understand such site preferences, a hypothetical "$Ca_{30}Zn_{63}$" model was built on the basis of the structure of $Ca_{30}Li_{3.44}Zn_{59.56}$ by placing zinc at the icosahedral center and both M3 and M5 sites. Mulliken populations (MPs) as a function of the VEC were calculated using the semiempirical EHTB method. Relative MPs were obtained by subtracting the MP at a specific site from the average MP of all sites for a given VEC. This method has been developed by Miller[55] as a tool for "coloring" analyses and successfully applied to explain structural or site preferences for many intermetallic systems.[55−58]

Figure 4 shows variation of the difference between the MP at each Zn site and the average MP of all Zn sites (or the relative MP) as a function of the VEC. Around the observed VEC range of 182−183, the site occupied by a Li atom has the most positive relative MP compared to all other Zn sites; the M5 and M3 sites are slightly more positive than the Zn1, Zn2, Zn4, and Zn6 sites, all of which have negative relative MPs. These results suggest that Li, M5, and M3 sites prefer more electropositive (less electron-rich) elements compared to other Zn sites, consistent with the absolute Mulliken electronegativities of Li and Zn sites (3.01 vs 4.45 eV).[59]

Other Phases with Similar Structural Motifs. Only a limited number of phases with similar structural motifs have been reported in the literature; these are listed in Table 2. The major differences among the first 10 phases lie in (1) the occupation of the icosahedral center and (2) various splitting patterns in tunnels defined by *arachno*-M_{18} clusters. These variations result in different Pearson symbols of *hP*90−93 (Note: $Ca_{24.7}Yb_{6.7}Ni_9Zn_{54}$ was wrongly noted as *hP*94 in the ICSD database; it should be *hP*93), and all phases have a narrow range of $c/a \approx 0.601-0.612$. In comparison, $Na_6Mg_{24}Ga_{55.2}$ exhibits a modified structure (Pearson symbol *hP*84),[60] in which the waist atoms of the *archano*-M_{18} cluster are missing, leading to a smaller c/a value of 0.583 and more split sites within the tunnels, on icosahedra, and on defect *arachno*-M_{18} clusters. There are two other germane phases ($Na_5Sn_{0.5}Ga_{8.5}$ and KIn_xCd_{2-x})[39] briefly mentioned in the literature, but no crystallographic data are available.

Three subclasses can be identified among the first 10 phases on the basis of VECs. One subclass includes the first three zinc-containing compositions, with VEC ∼ 182.5−188.8 e^-/cell. The components of this group mainly derive from an alkaline-earth metal (Ca) and a group 12 element (Zn) in a ratio of about 1:2, together with a minor component of lithium. The structures of this group feature fully Li/Ni-centered icosahedra. The second subclass includes four sodium-containing phases ($Na_8K_{23}Cd_{12}In_{48}$,[61] $Na_{30.5}Ag_{6.4}Ga_{53.6}$,[10] $Na_{30.5}Ag_{2.6}Ga_{57.4}$,[39] and $Na_{30.1}Au_{3.4}Ga_{56.6}$[40]), with VEC = 197.7−205.3 e^-/cell. These phases are dominated by alkali metal(s) and a group 13 element, also in a ratio of about 1:2, together with a minor component from a group 11 or 12 metal. However, icosahedral centers in these structures are exclusively empty. The third subclass includes three phases $Ba_{30.3}Li_{33.6}In_{29.4}$,[62] $Ca_{30}Cu_{29.46}Al_{33.68}$,[63] and $Ca_{30}Cu_{25.0}Al_{38.0}$,[50] which contain an alkaline-earth metal, a monovalent alkali or group 11 metal, and a group 13 metals in a ratio of about 1:1:1. The VEC range of

dx.doi.org/10.1021/ic502326j | Inorg. Chem. 2015, 54, 922−929

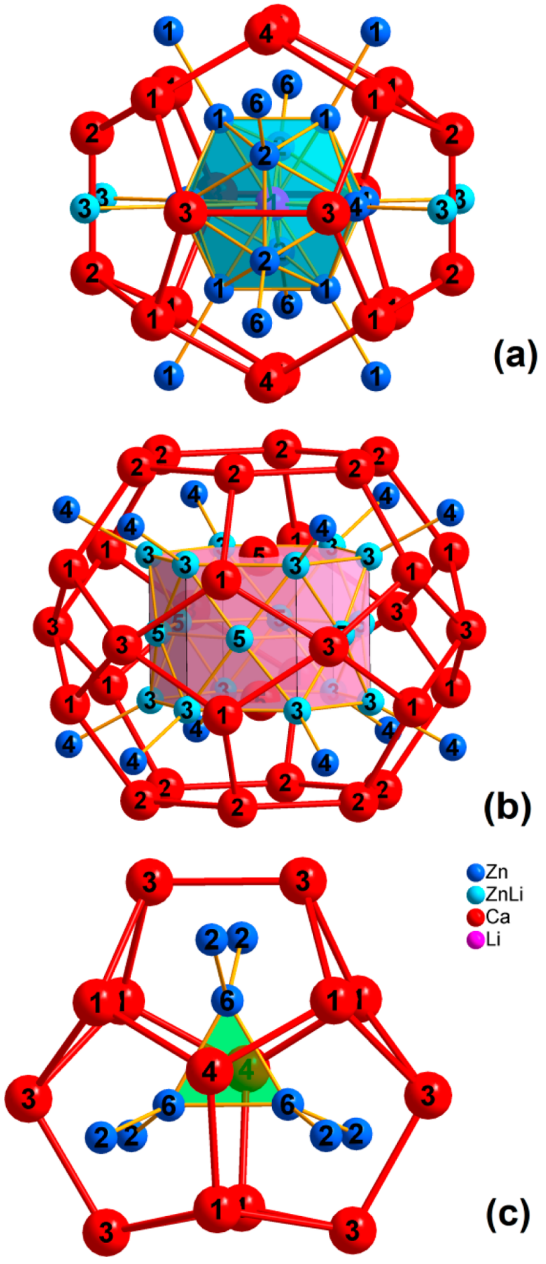

Figure 3. Endohedral clusters of (a) a Li@Zn_{12} icosahedron (turquoise) in a Ca_{20} dodecahedron (5^{12}), (b) a M_{18} tubular cluster (rose) in a Ca_{30} polyhedron ($3^{12}5^{12}6^2$), and (c) a Zn_3 triangle (green) in a Ca_{14} polyhedron (3^65^6) in the structure of **1**. The numbers denote atoms, as listed in Table 2.

this group lies between the foregoing two groups, 182.4−199.0, and the centers of icosahedra are also occupied. Apparently, the size factor plays an important role in determining whether the icosahedra are occupied or not. It appears that only Li, Cu, or Ni (with suitable sizes and s^{1-2} configurations) can occupy the centers of icosahedra, whereas other slightly larger elements with s^1, e.g., Na, Ag, or s^2 configurations, e.g., Zn, do not. According to experimental results (above), Cu could not replace Li in the title phase, probably because of a mismatch in size, as indicated by r_{ico} values in Table 2.

Valence Electron Counting. Table 3 gives the electron counting scheme for the title phase using electron counting approaches of Wade−Mingos.[6,7] The results of extended Hückel MO calculations for the isolated Li@$Zn_{12}H_{12}^{-13}$ and

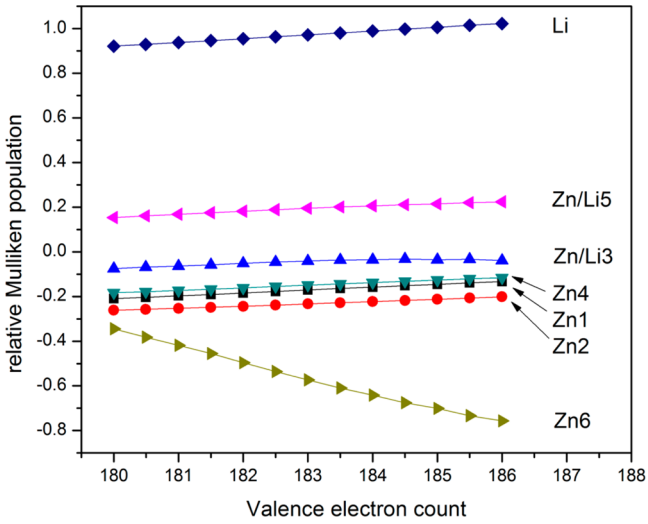

Figure 4. Relative MPs of Li and Zn sites in a hypothetical "$Ca_{30}Zn_{63}$" model as a function of the VEC.

$Zn_{18}H_{12}^{-18}$ clusters are given in the SI (Figure S1). In agreement with Wade's $(2n + 2)$ formula for skeletal electron counting, the Li@Zn_{12} icosahedron (a *closo* polyhedron) requires 26 skeletal electrons below a gap of ca. 1.0 eV. Upon including its 12 exobonded electrons, a total of 38 valence electrons are required for stabilization of the cluster. For the *arachno*-M_{18} polyhedron, a total of 42 skeletal electrons are required according to MO calculation of the $Zn_{18}H_{12}^{-18}$ cluster (Figure S1 in the SI). This value also agrees with Wade's rules $(2n + 6)$ for the number of skeletal electrons of an *arachno* polyhedron. So, a total of 42 + 12 = 54 bonding electrons are required, including its 12 exobonds. In the Zn_3 triangular cluster, each Zn atom can be viewed as a four-bonded bridging atom, as treated for the Ga_3 cluster in $Na_{30.5}Ag_{6.4}Ga_{53.6}$[39] and In_3 in $Na_8K_{23}Cd_{12}In_{48}$.[9] Thus, each Zn_3 triangular cluster needs two more valence electrons to fulfill a closed shell (octet rule), giving a total of six electrons for each Zn_3 unit. As a result, a total of 180 bonding electrons is necessary to stabilize the structure, about 2.6 electrons less than that provided by refined compositions. Therefore, the title compounds do not have closed-shell electronic structures but are slightly valence-electron-excessive, consistent with the metallic character confirmed by resistivity measurements (Figure S2 in the SI).

On the basis of the foregoing electron counting (Table 3), the formal charges for Li@Zn_{12} and Zn_{18} clusters are 13− and 18−, respectively, and each Zn_3 triangular cluster has a total formal charge of 6−, so the total charge for the condensed network of Zn clusters is 69− [=3(13−) + (18−) + 2(6−)]. Although the negative charge can be slightly decreased by

Table 3. Electron Counting for $Ca_{30+\Delta}Li_{3+x}Zn_{60-x}$ (x = 0.44−1.38)

	skeleton	exobond	total
Li@Zn_{12} icosahedron	2 × 12 + 2 = 26	12	38
arachno-M_{18} polyhedron	2 × 18 + 6 = 42	12	54
four bonded zinc in Zn_3	2 × 3 = 6		6
bonding electrons required	54 × 1 + 38 × 3 + 6 × 2 = 180		
electrons provided by components	182.56−182.62		
difference/cell	2.56−2.62		

dx.doi.org/10.1021/ic502326j | *Inorg. Chem.* 2015, 54, 922−929

allowing Zn/Li alloying, it is still about 8−9 more negative than what Ca atoms can donate (60−60.9 e^+). A similar situation also occurs for $Na_8K_{23}Cd_{12}In_{48}$[8] and $Na_{30.5}Ag_{6.4}Ga_{53.6}$.[12] To understand such a disagreement, a discussion using a more accurate electronic structure of the title phase is performed below.

Electronic Structure. Figure 5a shows the total and projected density of states (DOS) curves of a disorder-free

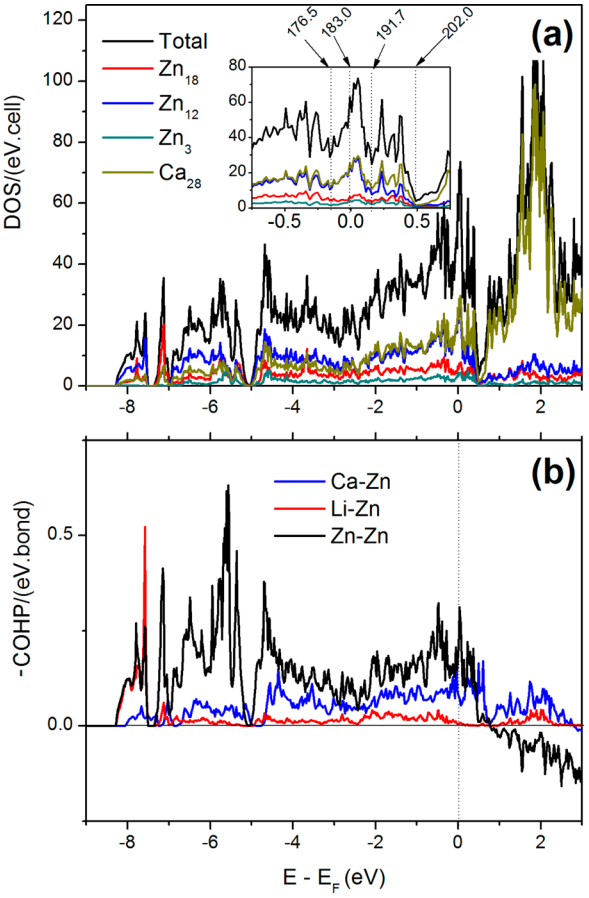

Figure 5. (a) Total and projected DOS and (b) COHP for "$Ca_{30}Li_3Zn_{60}$".

"$Ca_{30}Li_3Zn_{60}$" model calculated by the TB-LMTO-ASA method. The total DOS is a continuous curve across the Fermi energy (E_F); thus, the title phase is predicted to be a poor metal, consistent with its resistivity measurement (7.4×10^{-5} Ω cm at 293 K; Figure S2 in the SI). The Fermi levels for refined compositions (VEC = 182.4−182.5) are located at about −0.01 eV, corresponding to a small ditch on the plateau located to the left side of the large DOS at E_F. This indicates that a composition with slightly lower VEC than that of "$Ca_{30}Li_3Zn_{60}$" remains electronically stable, whereas a composition with larger VEC is not favorable in energy. This could explain why only very small lithium percentages can be alloyed with zinc. However, this type of structure could, under rigid band assumptions, accept up to a VEC of 202 electrons without noticeable destabilization because the extra electrons would fill states that are still bonding (see Figure 5b). Also, this result has been demonstrated by those phases dominated by Al, Ga, or In listed in Table 2.

As shown in the inset of Figure 5a, several deep valleys or pseudogaps occur in the DOS within the VEC range of 176.5−202.0. In all cases, however, the clathrate-like Ca_{28} framework has significant contributions (mainly 3d character; see Figure S3 in the SI) to the total DOS, suggesting an important role of the participation of Ca 3d orbitals in polar covalent bonding. The latter is also supported by the remarkably large contribution (41.0%) of Ca−Zn bond interactions to the total bond population, as evaluated by integrated COHP data, i.e., −ICOHP values (Table 4). This percentage is about 2.4

Table 4. Bond Length Ranges and Average −ICOHP Values for Hypothetical "$Ca_{30}Li_3Zn_{60}$" and "$Na_{30}Ga_{60}$"

bond type	length (Å)	−ICOHP (eV/ave bond)	multiplicity	−ICOHP (eV/cell)	contribution (%)
		$Ca_{30}Li_3Zn_{60}$			
Zn−Zn	2.585−3.017	1.27	156	198.1	53.7
Li−Zn	2.576−2.704	0.20	36	7.2	1.9
Ca−Zn	3.161−3.452	0.45	336	151.2	41.0
Ca−Ca	3.425−3.961	0.19	66	12.5	3.4
		$Na_{30}Ga_{60}$			
Ga−Ga	2.597−2.986	1.63	156	254.3	82.0
Na−Ga	3.068−3.452	0.16	336	53.8	17.3
Na−Na	3.368−3.71	0.03	66	2.0	0.7

times the contribution of Na−Ga bonds in "$Na_{30}Ga_{60}$", a model built from the structure of isostructural $Na_{30.5}Ag_{6.4}Ga_{53.6}$.[39] Apparently, the difference between the formal negative charge of the zinc network and the formal positive charge from calcium can be smeared out by the pronounced covalent interactions. In other words, the present phase may be referred to as a Zintl-like polar phase with an open-shell electronic structure.

CONCLUSIONS

In this work, the first ternary phase in the Ca−Li−Zn system, $Ca_{\sim 30}Li_{3+x}Zn_{60-x}$ (x = 0.44−1.38), exhibiting a remarkably condensed network of Zn_3, Zn_{12}, and Zn_{18} clusters, was synthesized and structurally characterized by single-crystal XRD. The phase can be obtained by lithiation of $CaZn_2$, which contains a three-dimensionally distorted tetrahedral framework of Zn atoms. Arguably, the structure of this Zintl-like phase may be established by valence electron counting approaches of Wade−Mingos rules on polyhedral clusters. The disagreement is incurred by the strong polar−covalent interactions between calcium and the zinc network of clusters. A better knowledge of zinc cluster chemistry in intermetallics could, in turn, help to better understand the formation of dendrites in zinc batteries. The study of the influence of lithium on zinc clustering of other Ca/Zn ratios and on transition metal−zinc systems is still ongoing.

ASSOCIATED CONTENT

Supporting Information

Atomic coordinates and equivalent isotropic displacement parameters for crystals **1** and **2** (Table S1), selected important interatomic distances in **1**, together with the respective −ICOHP values (Table S2), MO diagrams for Li@$Zn_{12}H_{12}^{13-}$ and $Zn_{18}H_{12}^{18-}$ clusters (Figure S1), resistivity

dx.doi.org/10.1021/ic502326j | Inorg. Chem. 2015, 54, 922−929

data for $CaZn_2$ and "$Ca_{30}Li_5Zn_{60}$" (Figure S2), partial DOS of calcium in "$Ca_{30}Li_3Zn_{60}$" (Figure S3), and a CIF file. This material is available free of charge via the Internet at http://pubs.acs.org.

AUTHOR INFORMATION

Corresponding Author

*E-mail: qslin@ameslab.gov.

Notes

The authors declare no competing financial interest.

ACKNOWLEDGMENTS

Thanks go to Dr. T. Valentin from Ames Laboratory for resistivity measurements. The research was supported by the Office of the Basic Energy Sciences, Materials Sciences Division, U.S. Department of Energy (DOE). Ames Laboratory is operated for the DOE by Iowa State University under Contract DE-AC02-07CH11358.

REFERENCES

(1) Corbett, J. D. *Chem. Rev.* **1985**, *85*, 383−397.
(2) Corbett, J. D. *Angew. Chem., Int. Ed.* **2000**, *39*, 670−690.
(3) Simon, A. *Philos. Trans. R. Soc., A* **2010**, *368*, 1285−1299.
(4) Svensson, G.; Koehler, J.; Simon, A. In *Metal Clusters in Chemistry*, Braunstein, P., Oro, L. A., Raithby, P. R., Eds.; Wiley-VCH: Weinheim, Germany, 1999; Vol. 3, pp 1509−1550.
(5) Kauzlarich, S. M. *Chemistry, Structure, and Bonding of Zintl Phases and Ions*; VCH: New York, 1996.
(6) Wade, K. *Adv. Inorg. Chem. Radiochem.* **1976**, *18*, 1−66.
(7) Mingos, D. M. P. *J. Chem. Soc., Chem. Commun.* **1983**, 706−708.
(8) Schäfer, H.; Eisenmann, B.; Müller, W. *Angew. Chem., Int. Ed.* **1973**, *12*, 694−712.
(9) Klemm, W.; Busmann, E. *Z. Anorg. Allg. Chem.* **1963**, *319*, 297−311.
(10) Perrin, C. In *Metal Clusters in Chemistry*; Braunstein, P., Oro, L. A., Raithby, P. R., Eds.; Wiley-VCH: Weinheim, Germany, 1999; Vol. 3, pp 1563−1590.
(11) Moore, C. E. *Atomic Energy Levels*; National Bureau of Standards: Washington DC, 1971.
(12) Viklund, P.; Svensson, C.; Hull, S.; Simak, S. I.; Berastegui, P.; Häußermann, U. *Chem.—Eur. J.* **2001**, *7*, 5143−5152.
(13) Villars, P.; Calvert, L. D. *Pearson's Handbook of Crystallographic Data for Intermetallic Phases*, 2nd ed.; American Society of Metals: Materials Park, OH, 1991; Vol. 1.
(14) Lin, Q.; Corbett, J. D. *Philos. Mag. Lett.* **2003**, *83*, 755−762.
(15) Lin, Q.; Corbett, J. D. *Inorg. Chem.* **2004**, *43*, 1912−1919.
(16) Lin, Q.; Corbett, J. D. *J. Am. Chem. Soc.* **2006**, *128*, 13268−13273.
(17) Lin, Q.; Corbett, J. D. *Proc. Natl. Acad. Sci. U.S.A.* **2006**, *103*, 13589−13594.
(18) Pay Gómez, C.; Lidin, S. *Angew. Chem., Int. Ed.* **2001**, *40*, 4037−4039.
(19) Pay Gómez, C.; Lidin, S. *Phys. Rev. B* **2003**, *68*, 024203/1−9.
(20) Piao, S.; Gomez, C. P.; Lidin, S. *Z. Naturforsch.* **2006**, *61B*, 644−649.
(21) Piao, S.; Lidin, S. *Inorg. Chem.* **2007**, *46*, 6452−6463.
(22) Piao, S. Y.; Palatinus, L.; Lidin, S. *Inorg. Chem.* **2008**, *47*, 1079−1086.
(23) Lin, Q.; Corbett, J. D. *Struct. Bonding (Berlin)* **2009**, *133*, 1−39.
(24) Tsai, A. P.; Guo, J. Q.; Abe, E.; Takakura, H.; Sato, T. J. *Nature* **2000**, *408*, 537−538.
(25) Samal, S. L.; Lin, Q.; Corbett, J. D. *Inorg. Chem.* **2012**, *51*, 9395−402.
(26) Samal, S. L.; Corbett, J. D. *Inorg. Chem.* **2011**, *50*, 7033−7039.
(27) Samal, S. L.; Gulo, F.; Corbett, J. D. *Inorg. Chem.* **2013**, *52*, 2697−2704.
(28) Gulo, F.; Samal, S. L.; Corbett, J. D. *Inorg. Chem.* **2013**, *52*, 10112−10118.
(29) Rahman, M. A.; Wang, X.; Wen, C. *J. Electrochem. Soc.* **2013**, *160*, A1759−A1771.
(30) Toussaint, G.; Stevens, P.; Akrour, L.; Rouget, R.; Fourgeot, F. *ECS Trans.* **2010**, *28*, 25−34.
(31) Drillet, J.-F.; Adam, M.; Barg, S.; Herter, A.; Koch, D.; Schmidt, V.; Wilhelm, M. *ECS Trans.* **2010**, *28*, 13−24.
(32) Iokibe, K.; Tachikawa, H.; Azumi, K. *J. Phys. B: At., Mol. Opt. Phys.* **2007**, *40*, 427.
(33) Wang, J.; Wang, G.; Zhao, J. *Phys. Rev. A* **2003**, *68*, 013201/1−6.
(34) Stojanovic, M.; Latturner, S. E. *J. Solid State Chem.* **2009**, *182*, 2239−2245.
(35) *SAINT plus*, version 8.30; Bruker AXS Inc.: Madison, WI, 2013.
(36) Sheldrick, G. M. *SADABS*; University of Göttingen: Göttingen, Germany, 1996.
(37) *SHELXTL*, 6.10 ed.; Bruker Analytical X-ray Systems, Inc.: Madison, WI, 2000.
(38) Palatinis, L.; Chapuis, G. *J. Appl. Crystallogr.* **2007**, *40*, 786−790.
(39) Henning, R. W.; Corbett, J. D. *Z. Anorg. Allg. Chem.* **2002**, *628*, 2715−2723.
(40) Smetana, V.; Miller, G. J.; Corbett, J. D. *Inorg. Chem.* **2013**, *52*, 12502−12510.
(41) Tank, R.; Jepsen, O.; Burkhardt, A.; Andersen, O. K. *TB-LMTO-ASA Program*, version 4.7; Max-Planck-Institut für Festkörperforschung: Stuttgart, Germany, 1994.
(42) Shriver, H. L. *The LMTO Method*; Springer-Verlag: Berlin, 1984.
(43) Andersen, K.; Jepsen, O. *Phys. Rev. Lett.* **1984**, *53*, 2571−2574.
(44) Dronskowski, R.; Bloechl, P. E. *J. Phys. Chem.* **1993**, *97*, 8617−8624.
(45) Ren, J.; Liang, W.; Whangbo, M.-H. *CAESAR for Windows*; Prime-Color Software, Inc. and North Carolina State University: Raleigh, NC, 1998.
(46) Mel'nik, E. V.; Kripyakevich, P. I. *Kristallografiya* **1974**, *19*, 645−646.
(47) Li, B.; Corbett, J. D. *J. Am. Chem. Soc.* **2006**, *128*, 12392−12393.
(48) Corbett, J. D. *Inorg. Chem.* **2000**, *39*, 5178−5191.
(49) Lin, Q.; Lidin, S.; Corbett, J. D. *Inorg. Chem.* **2007**, *47*, 1020−1029.
(50) Zarechnyuk, O. S.; Manyako, N. B.; Yanson, T. I.; Bruskov, V. A. *Kristallografiya* **1988**, *33*, 336−40.
(51) Jeffrey, G. A. In *Inclusion Compounds*; Atwood, J. L., Davies, J. E. D., MacNicol, D. D., Eds.; Academic Press: London, 1984; pp 135−188.
(52) Pauling, L. *The Nature of the Chemical Bond*, 3rd ed.; Cornell University Press: Ithaca, NY, 1960; p 644.
(53) Zintl, E.; Schneider, A. *Z. Elektrochem. Angew. Phys. Chem.* **1935**, *41*, 764−767.
(54) Bergman, G.; Waugh, J. L. T.; Pauling, L. *Acta Crystallogr.* **1957**, *10*, 254.
(55) Miller, G. J. *Eur. J. Inorg. Chem.* **1998**, 523−536.
(56) Li, B.; Corbett, J. D. *Inorg. Chem.* **2004**, *43*, 3582−3587.
(57) Mishra, T.; Lin, Q.; Corbett, J. D. *J. Solid State Chem.* **2014**, *218*, 103−108.
(58) Lin, Q.; Miller, G. J.; Corbett, J. D. *Inorg. Chem.* **2014**, *53*, 5875−5877.
(59) Pearson, R. G. *Inorg. Chem.* **1988**, *27*, 734.
(60) Nesper, R. *Angew. Chem., Int. Ed.* **1989**, *28*, 58−59.
(61) Flot, D. M.; Tillard-Charbonnel, M. M.; Belin, C. H. E. *J. Am. Chem. Soc.* **1996**, *118*, 5229−5235.
(62) Smetana, V.; Vajenine, G. V.; Kienle, L.; Duppel, V.; Simon, A. *J. Solid State Chem.* **2010**, *183*, 1767−1775.
(63) Fornasini, M. L.; Merlo, F. *Acta Crystallogr., Sect. C* **1988**, *44*, 1351−1355.